CHEMISTRY OF MATERIALS
Article

Chem. Mater. **2010,** *22,* 467–475 467
DOI:10.1021/cm903282w

Novel Nanocrystalline $Ce_{1-x}La_xO_{2-\delta}$ ($x = 0.2$) Solid Solutions: Structural Characteristics and Catalytic Performance

Benjaram, M. Reddy,* Lakshmi Katta, and Gode Thrimurthulu

Inorganic and Physical Chemistry Division, Indian Institute of Chemical Technology, Uppal Road, Hyderabad - 500 607, India

Received October 27, 2009. Revised Manuscript Received December 15, 2009

The catalytic CO oxidation results revealed that nanosized ceria-lanthana (CL) solid solution exhibits superior catalytic performance and thermal stability in comparison to ceria-zirconia (CZ) solid solution. The rationale for excellent catalytic behavior of the CL sample was elucidated from the viewpoint of structure, redox behavior, and bulk oxygen mobility. Accordingly, in this investigation CL solid solution has been synthesized by a modified coprecipitation method, and the structural and redox properties have been deeply investigated employing various characterization techniques, namely, X-ray diffraction (XRD), BET surface area, transmission electron microscopy (TEM), Raman spectroscopy (UV-RS and Vis-RS), UV-visible diffuse reflectance spectroscopy (UV-vis DRS), and temperature programmed reduction (TPR). The catalytic efficiency has been evaluated for oxygen storage/release capacity (OSC) and CO oxidation activity. The analyses of the characterization results provided a deep insight on the physical properties like nanocrystalline nature and surface area, and the chemical properties like oxygen deficiency and reducibility. The lattice parameter of the cubic phase has been observed to increase because of the formation of a solid solution of the type $Ce_{1-x}La_xO_{2-\delta}$ ($x = 0.2$) due to partial substitution of La^{3+} into CeO_2 lattice. A correlation is found between the concentration of Ce^{3+}, lattice defects, and oxygen migration rate with the OSC and reducibility. The detailed investigation infers that the CL solid solution exhibits better catalytic properties due to smaller crystallite size, facile reduction, profound bulk oxygen mobility, and enhanced OSC.

1. Introduction

The progressive deterioration of quality of human health is attributed to the environmental pollution. In the emerging field of nanotechnology, the primary goal of many investigations is to synthesize nanomaterials with desired functional properties. From the environmental point of view, the design of some specific nanomaterials (TiO_2, ZnS, Fe(0), CeO_2, etc.) has received much attention in the recent past since these materials are expected to remediate such type of problems.[1] As a typical kind of rare earth oxide, ceria (CeO_2) has been extensively used as an active component in three-way catalysis (TWCs) where pollutant emissions from internal combustion engines are effectively reduced.[2−4] The reason for extensive use of ceria as an active ingredient in the TWCs applications is acknowledged from the nature of outstanding redox behavior being amenable for absorbing and giving off the oxygen from the atmosphere, which is known as oxygen storage/release capacity (OSC).[5−9] This unique property of ceria has been triggered off many salient applications of industrial significance.[10−12]

Although ceria has been studied extensively, under elevated conditions ceria becomes inefficient with time and many innate properties will be affected.[2,6] Hence, ceria is combined with other metal ions to make solid solutions with improved properties. Modification of ceria is a key issue in the development of efficient catalyst formulations for treatment of auto exhaust processes and other applications. The doped ceria enhances the surface area and can sustain toward sintering during the high temperature long-term anneal due to the cooperative

*Author to whom correspondence should be addressed. Phone: +91 40 2719 1714. Fax: +91 40 2716 0921. E-mail: bmreddy@iict.res.in, mreddyb@yahoo.com.

(1) Sunstrom, J. E.IV; Moser, J. E.; Marshik-Guerts, B. *Chem. Mater.* **1996**, *8*, 2061.
(2) Masui, T.; Peng, Y.; Machida, K.-I.; Adachi, G.-Y. *Chem. Mater.* **1998**, *10*, 4005.
(3) Luo, M.; Chen, J.; Chen, L.; Lu, J.; Feng, Z.; Li, Z. *Chem. Mater.* **2001**, *13*, 197.
(4) Balducci, G.; Kašpar, J.; Fornasiero, P.; Graziani, M.; Islam, M. S.; Gale, J. D. *J. Phys. Chem. B* **1997**, *101*, 1750.
(5) López-Haro, M.; Aboussaïd, K.; Gonzalez, J. C.; Hernández, J. C.; Pintado, J. M.; Blanco, G.; Calvino, J. J.; Midgley, P. A.; Bayle-Guillemaud, P.; Trasobares, S. *Chem. Mater.* **2009**, *21*, 1035.
(6) Balducci, G.; Saiful Islam, M.; Kaspar, J.; Fornasiero, P.; Graziani, M. *Chem. Mater.* **2000**, *12*, 677.
(7) Dong, L.; Hu, Y.; Shen, M.; Jin, T.; Wang, J.; Ding, W.; Chen, Y. *Chem. Mater.* **2001**, *13*, 4227.
(8) Dutta, G.; Waghmare, U. V.; Baidya, T.; Hegde, M. S.; Priolkar, K. R.; Sarode, P. R. *Chem. Mater.* **2006**, *18*, 3249.
(9) Liu, X.; Zhou, K.; Wang, L.; Wang, B.; Li, Y. *J. Am. Chem. Soc.* **2009**, *131*, 3140.
(10) Zou, H.; Lin, Y. S.; Rane, N.; He, T. *Ind. Eng. Chem. Res.* **2004**, *43*, 3019.
(11) Gu, H.; Soucek, M. D. *Chem. Mater.* **2007**, *19*, 1103.
(12) Yuan, Q.; Liu, Q.; Song, W.-G.; Feng, W.; Pu, W.-L.; Sun, L.-D.; Zhang, Y.-W.; Yan, C.-H. *J. Am. Chem. Soc.* **2007**, *129*, 6698.

Published on Web 12/30/2009

nature of the cations of the mixed oxides.[13,14] Further, the combination of different cations in the oxide matrix can produce materials with novel properties (structural or electronic properties) which may lead to high catalytic activity. Accordingly, ceria has been studied using a wide range of transition and rare-earth ions (variable and invariable valent cations) as additives since the host lattice of ceria is compatible with various substitutions.[3,15−17] The dopant ion obviously plays a crucial role in modifying the chemical and physical properties of the produced mixed oxides. For instance, the concentration of oxygen vacancies depends on the oxidation state of the dopant ion and the mobility of the oxygen vacancy/oxide ion depends on the association energy of the dopant ion with the oxygen vacancy. If the additive is aliovalent cation then the oxygen vacancies can be introduced due to charge compensation mechanism and thus OSC increases. On the other hand, for isovalent cation the oxygen vacancy/oxide ion migration aids from the strain and distortion due to mismatch of the ionic radius of the dopant and Ce-ions in the substituted sample. The problem with isovalent cation, especially with Zr^{4+} is that it induces very limited concentration of oxygen vacancies.[18] Therefore, the oxygen vacancy concentration and concomitant oxide ion conductivity can be increased through the lower-valent metal ion substitution. However, divalent dopant ions like Ca^{2+} incorporated samples are thermally less stable and prone to phase segregation due to significant drop in the strain and increase in the activation energy for the oxide ion/oxygen vacancy migration owing to defect association.[18−21] Whereas, undersized trivalent ions like Fe^{3+} are difficult to soluble in ceria lattice cell by traditional methods.[22,23] Interestingly, some investigations demonstrated that anion vacancies in the materials are weakly associated with dopant cations and does not lead to any superstructures.[24−27] According to M. F. Wilkes and coauthors, the optimum concentration for doping of bulk ceria is 12.5−25% so that the cubic structure will be retained.[26] Cubic structures, which consist sufficient channel size for the oxygen migration, is favorable for the OSC.

The present investigation was undertaken against the aforesaid background. Accordingly, an attempt has been made to integrate the synthesis, physicochemical characteristics, and catalytic efficiency of ceria-lanthana (CL) solid solutions. Method of preparation plays a significant role in modifying the thermal and redox properties, particularly when one of them is a minor component. Therefore, the investigated $CeO_2-La_2O_3$ (80:20) nanosized solid solutions were synthesized by a modified coprecipitation method which facilitates reasonably high specific surface area, homogeneous distribution of metal oxides in the bulk, and good thermal stability.[28] Various characterization techniques, namely, X-ray diffraction (XRD), BET surface area, transmission electron microscopy (TEM), Raman spectroscopy (UV-RS and Vis-RS), UV-visible diffuse reflectance spectroscopy (UV-vis DRS), and temperature programmed reduction (TPR) were employed for gaining insight into many of the physical and chemical properties of the synthesized materials. To assess the suitability of CL for TWC, these samples were evaluated for OSC and CO oxidation activity. The activity results of CL sample were compared with the ceria-zirconia (CZ) mixed oxide as it is a well established material in the TWC technology.

2. Experimental Section

2.1. Catalyst Preparation. The $CeO_2-La_2O_3$ (8:2 mol ratio based on oxides) solid solution was synthesized by a modified coprecipitation method from ultrahigh dilute solutions. This method is more attracting because of its relative simplicity, environmental friendliness, economical effectiveness, and suitability for large scale production.[29] Coprecipitation was carried out from $Ce(NO_3)_3 \cdot 6H_2O$ (Aldrich, AR grade) and $La(NO_3)_3 \cdot 6H_2O$ (Aldrich, AR grade) precursors, and a dilute aqueous ammonia solution was used as the precipitating agent. The requisite quantities of precursors were dissolved separately in double distilled water and mixed together under continuous stirring. The mixed solution was precipitated by dropwise addition of the aqueous ammonia solution over a period until the solution pH reached ~8.5. The obtained light yellow colored slurry was decanted, filtered, and washed several times with doubly distilled water until free from anion impurities. The collected precipitate was oven-dried at 393 K for 12 h, crushed using an agate mortar, and subsequently calcined at 773 K for 5 h at a heating rate of 5 K min^{-1} in air atmosphere to obtain the mixed oxide material. Finally, some portions of the finished catalyst were further heated at 873, 973, and 1073 K for 5 h using the same heating ramp.

2.2. Catalyst Characterization. Powder X-ray diffraction data were acquired on a Rigaku Multiflex instrument equipped with nickel-filtered Cu Kα (0.15418 nm) radiation source and a scintillation counter detector. The step size and the time per step were, respectively, fixed at 0.02° and 1 s in the range of 12−80°. The XRD phases present in the samples were identified with the help of Powder Diffraction File-International Center for

(13) Li, H.; Zhang, L.; Dai, H.; He, H. *Inorg. Chem.* **2009**, *48*, 4421.
(14) Wang, R.; Crozier, P. A.; Sharma, R.; Adams, J. B. *J. Phys. Chem. B* **2006**, *110*, 18278.
(15) Alifanti, M.; Baps, B.; Blangenois, N.; Naud, J.; Grange, P.; Delmon, B. *Chem. Mater.* **2003**, *15*, 395.
(16) Shan, W.; Shen, W.; Li, C. *Chem. Mater.* **2003**, *15*, 4761.
(17) Natile, M. M.; Glisenti, A. *Chem. Mater.* **2005**, *17*, 3403.
(18) García, M. F.; Arias, A. M.; Hanson, J. C.; Rodriguez, J. A. *Chem. Rev.* **2004**, *104*, 4063.
(19) Huang, W.; Shuk, P.; Greenblatt, M. *Chem. Mater.* **1997**, *9*, 2240.
(20) Albero, J. S.; Reinoso, F. R.; Escribano, A. S. *J. Catal.* **2002**, *210*, 127.
(21) Wang, X.; Hanson, J. C.; Liu, G.; Rodriguez, J. A.; Juez, I. A.; Garcia, M. F. *J. Chem. Phys.* **2004**, *121*, 5434.
(22) Li, G.; Smith, R. L., Jr.; Inomata, H. *J. Am. Chem. Soc.* **2001**, *123*, 11091.
(23) Pérez-Alonso, F. J.; López Granados, M.; Ojeda, M.; Terreros, P.; Rojas, S.; Herranz, T.; Fierro, J. L. G.; Gracia, M.; Gancedo, J. R. *Chem. Mater.* **2005**, *17*, 2329.
(24) O'Neill, W. M.; Morris, M. A. *Chem. Phys. Lett.* **1999**, *305*, 389.
(25) Kharton, V. V.; Yaremchenko, A. A.; Naumovich, E. N.; Marques, F. M. B. *J. Solid State Electrochem.* **2000**, *4*, 243.
(26) Wilkes, M. F.; Hayden, P.; Bhattacharya, A. K. *J. Catal.* **2003**, *219*, 286.
(27) Belliére, V.; Joorst, G.; Stephan, O.; de Groot, F. M. F.; Weckhuysen, B. M. *J. Phys. Chem. B* **2006**, *110*, 9984.
(28) Yuzhakova, T.; Rakic, V.; Guimon, C.; Auroux, A. *Chem. Mater.* **2007**, *19*, 2970.
(29) Taniguchi, T.; Watanabe, T.; Sakamoto, N.; Matsushita, N.; Yoshimura, M. *Cryst. Growth Des.* **2008**, *8*, 3725.

Diffraction Data (PDF-ICDD). The mean crystallite size of the solid solution phases was estimated with the help of Scherrer equation from line broadening, and the lattice parameter was calculated by a standard cubic indexation method using the intensity of the most prominent peak (111). The Raman spectra were obtained at room temperature using a LabRam HR800UV Raman spectrometer (Horiba Jobin-Yvon) fitted with a confocal microscope and liquid-nitrogen cooled charge-coupled device (CCD) detector. Samples were excited either with 325 nm of a He−Cd laser (Melles Griot Laser) or with the emission line at 632.81 nm from an Ar^+ ion laser (Spectra Physics) which was focused on the sample under the microscope with the diameter of the analyzed spot being ~1 μm. The acquisition time was adjusted according to the intensity of Raman scattering. The wavenumber values reported from the spectra are accurate to within 1 cm^{-1}.

Specific surface areas of the samples were determined by a single point BET analysis of the nitrogen adsorption isotherms at liquid N_2 temperature (77 K) recorded on a SMART SORB-92/93 instrument via a thermal conductivity detector (TCD). Prior to the experiment, samples were degassed at 393 K for 2 h to remove any surface adsorbed residual moisture. Surface area is obtained by using the desorption data. The UV-vis DRS measurements were performed over the wavelength range of λ = 200−750 nm using a GBS-Cintra 10e UV-vis NIR spectrophotometer with an integration sphere diffuse reflectance attachment. Sample was diluted in a KBr matrix by pelletization. The TEM-HREM studies were made on a JEM-2010 (JEOL) instrument equipped with a slow-scan CCD camera and at an accelerating voltage of 200 kV. Samples for TEM were prepared by crushing the materials in an agate mortar and dispersing them ultrasonically in ethyl alcohol. After dispersion, a droplet was deposited on a copper grid supporting a perforated carbon film and allowed to dry. The specimen was examined under vacuum at room temperature.

The XPS analysis was performed using a Shimadzu (ESCA 3400) spectrometer. The X-ray source utilized was monochromatic Mg Kα (1253.6 eV) radiation. The analysis was done at room temperature and pressures were typically in the order of less than 10^{-8} Pa to avoid large amount of noise in the spectra from contaminates. Charging of the samples was minimized by referencing the spectra to the C 1s line at BE 284.6 eV.[30] Samples were outgassed overnight in a vacuum oven before XPS measurements. The surface compositions were determined from photoelectron peak areas using the atomic sensitivity factors following the Shirley background subtraction.[30] All binding energies measured were within a precision of ±0.2 eV.

Reducibility of the samples was examined by TPR using thermal conductivity detector of a gas chromatograph (Shimadzu) in a conventional apparatus. Approximately 30 mg of sample mass was loaded in an isothermal zone of the reactor and heated at a rate of 10 K min^{-1} to 473 K using 30 mL min^{-1} He gas flow which facilitated to drive away the molecules that had been preadsorbed on the surface of the sample. After the sample was cooled to room temperature, the He was switched to 5% H_2/Ar with a rate of 20 mL min^{-1} and the temperature was linearly raised to 1073 K at a continuous heating ramp of 5 K min^{-1}, keeping all the parameters unchanged. The hydrogen consumption during the reduction process was calculated by passing the effluent gas through a molecular sieve trap to remove the produced water and then to TCD.

2.3. Catalyst Evaluation. The OSC of the catalysts was determined using a thermogravimetry (TG) method by employing a commercial Netzsch TG-DTA (Luxx, STA, 409 PC, Germany) analyzer under repeated thermal treatments in the temperature window of 573−1073 K.[31] In this method, the OSC of the catalyst is measured in terms of the amount of oxygen released during heat treatments. The weight change during the thermal treatments was monitored by TG in flowing nitrogen or dry air. The heat cycle consisted of heating the sample to 1073 K, cooling to 423 K, and again heating to 1073 K. All heating and cooling rates were in the steps of 5 K min^{-1}. The weight loss of the sample during the second stage of heat treatment was used to measure the oxygen release properties.

The catalytic activity of the sample for oxidation of CO was conducted at normal pressure (one atmosphere) in the temperature range 300−773 K in a fixed bed microreactor under the temperature ramp of 5 K min^{-1}. Approximately 100 mg catalyst sample (250−355 μm sieve fraction) was diluted with quartz particles of the same sieve fraction and was placed in a quartz reactor and its ends plugged with ceramic wool. Reaction temperature was monitored using a thermocouple placed in the hollow part of the reactor. The following gases and gas mixtures were used (supplied by Air Liquide): argon (>99.999% purity), 9.98% CO (CO purity, >99.997%), and 10.2% O_2 (oxygen purity, >99.995%) with argon as balance. The total flow rates maintained by three mass flow controllers were in the range of 50−60 N mL min^{-1} (milliliters normalized to 273.15 K and 1 atm.). The CO and CO_2 gas concentrations were measured using an Uras 14 infrared analyzer module, and the O_2 concentration was measured using a Magnos 16 analyzer (Hartmann & Braun). Prior to oxidation of CO, the catalyst was heated to 773 K in 10.2% O_2/Ar gas mixture, using a heating ramp of 10 K min^{-1}, and kept at the final temperature for 1 h. The oxidized sample was then purged in argon to avoid gas phase reaction and cooled to the desired starting temperature. The CO/O_2 reactant feed ratio was 1, and partial pressures of CO and O_2 were in the range of 10 mbar.

3. Results and Discussion

The XRD patterns of ceria-lanthana solid solution calcined at various temperatures in the range of 773−1073 K along with pure ceria calcined at 773 K are shown in Figure 1. Detailed analysis revealed that all patterns are symmetric in nature and match well with the sole presence of the standard fluorite type cubic phase of CeO_2.[32] From the XRD patterns it could be noted that doping of CeO_2 with La^{3+} lead to shifting of diffraction peaks toward lower angle side and become broad with low intensity. Further, no peaks were observed corresponding to the individual oxides (La_2O_3 etc.). This disparate feature compared to pure ceria can be explained as due to the formation of CL solid solution. The formation of solid solution originates from the partial substitution of Ce^{4+} with La^{3+}. The ionic radius of La^{3+} (0.11 nm) is larger than Ce^{4+} (0.097 nm) hence lattice expansion is expected due to incorporation of La^{3+} into CeO_2 lattice. Relative to pure ceria (5.41 Å), the cell parameter "*a*"

(30) Wagner, C. D.; Riggs, W. M.; Davis, L. E.; Moulder, J. F. In *Handbook of X-ray Photoelectron Spectroscopy*; Muilenberg, G. E., Ed.; Perkin-Elmer Corporation: Eden Prairie, MN, 1978.

(31) Ozawa, M.; Matuda, K.; Suzuki, S. *J. Alloys Compd.* **2000**, *303−304*, 56.

(32) Wilkes, M. F.; Hayden, P.; Bhattacharya, A. K. *J. Catal.* **2003**, *219*, 305.

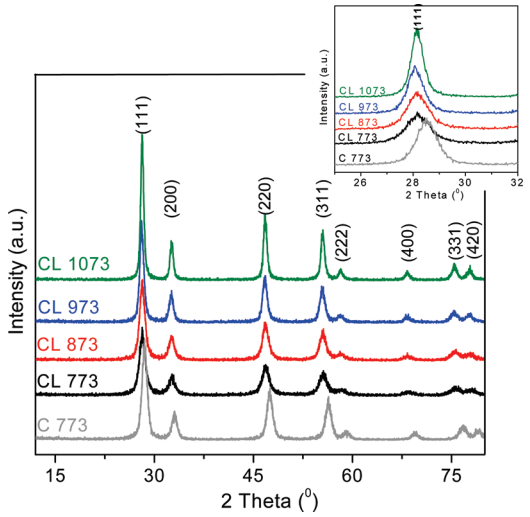

Figure 1. Powder X-ray diffraction patterns of pure ceria (C) and ceria-lanthana (CL) calcined at various temperatures from 773 to 1073 K.

Table 1. BET Surface Area, Average Crystallite Size, and Lattice Parameter "a" of Samples Calcined at Various Temperatures

sample	surface area (m^2g^{-1})	crystallite size (nm)[a]	lattice parameter (Å)[a]	OSC/μ moles O_2/g ceria
CeO_2 773	41	8.92	5.41	40.5
CeO_2 1073	8	32.5	5.41	
$CeO_2-La_2O_3$ 773	66	8.33	5.488	225
$CeO_2-La_2O_3$ 873	58	8.92	5.485	
$CeO_2-La_2O_3$ 973	47	12.28	5.508	
$CeO_2-La_2O_3$ 1073	40	15.67	5.492	

[a] From XRD analysis.

(calculated using the most prominent (111) line corresponding to 0.316 nm lattice spacing of the fluorite structure) of CL solid solution is increased to 5.49 ± 0.005 Å (1% lattice expansion is observed for 20% La^{3+} incorporation) as expected, and is in good agreement with the previous reports.[32,33] Textural and structural characterization data of CL sample calcined at various temperatures are presented in Table 1 together with the data of pure ceria (C 773). With increase in calcination temperature two important observations were distinctly reflected in the XRD results. (i) Crystallite size is increased due to the effect of sintering which is evidenced by a gain in the intensity and become better defined diffraction lines (inverse proportional of half width at half-maximum to the crystal diameter to the first power). (ii) No new phase except $Ce_{0.8}La_{0.2}O_{2-\delta}$ is observed which is confirmed by the consistency in the lattice parameter. Interestingly, despite the increase in the crystallite size no appreciable difference in the lattice parameter is noticed. This infers that the introduction of La^{3+} ions into CeO_2 can stabilize the host lattice at high temperatures.

The objective of XPS analysis was to investigate the valence states of the ingredients of the CL sample. The Ce 3d core level spectra of CL solid solutions are illustrated in Figure 2. The Ce 3d spectra are complex due to

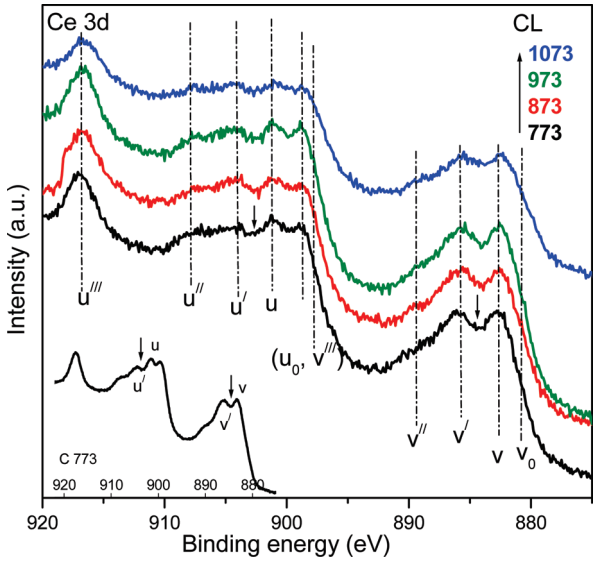

Figure 2. Ce 3d XP spectra of ceria-lanthana (CL) samples calcined at various temperatures from 773 to 1073 K.

spin−orbit coupling. The labels u and v refer to the spin orbit components assigned to 3/2 and 5/2, respectively. Observation of main peaks approximately at 917.0 and 885.7 eV describe the relative amount of Ce^{4+} and Ce^{3+} present in the sample, respectively. This emphasizes that both 3+ and 4+ oxidation states coexist in the sample. Compared to pure ceria the valley between v and v′ and/or u and u′ is low for CL solid solution, therefore, it is expected that conversion of $Ce^{4+} \rightarrow Ce^{3+}$ and thus oxygen vacancies are more, a similar observation was noticed by Ji et al. for ordered mesoporous ceria.[34] As calcination temperature increased, u′′′ peak intensity is decreased which could be also due to ultra high vacuum conditions during the XPS measurements. There is a probability that the conversion of $Ce^{4+} \rightarrow Ce^{3+}$ is possible under the vacuum in agreement with the earlier reports.[20]

Ce 4d XP core level spectra are shown in Figure 3. The study of Ce 4d core level peak is also expected to provide some additional piece of information on the electronic structure of the Ce. The band at ~123 eV is a reflection from the Ce $4d_{5/2}$ component aroused due to the contribution from Ce^{4+} ions. The band at ~103.3 eV is directly correlated to the proportion of Ce^{3+} component.[35] The presence of these two bands give evidence for Ce fluctuation between 3+ and 4+ oxidations. The slightly elevated and complex region extending from 117 to 105 eV is attributed to $4d^94f^1$ and $4d^94f^2$ final states.[36] The splitting pattern of La 3d core level spectra is depicted in Figure 4. The splitting is due to spin orbit interaction and charge transfer from ligand (O 2p) to the metal (La 4f). Splitting energy observed from the spectra is ~4.25 eV, which is also supported by earlier reports.[37] As can be

(33) Bueno-López, A.; Such-Basáñez, I.; de Lecea, C. S.-M. *J. Catal.* **2006**, *244*, 102.
(34) Ji, P.; Zhang, J.; Chen, F.; Anpo, M. *J. Phys. Chem. C* **2008**, *112*, 17809.
(35) Liu, G.; Rodriguez, J. A.; Chang, Z.; Hrbek, J.; Peden, C. H. F. *J. Phys. Chem. B* **2004**, *108*, 2931.
(36) Xiao, W.; Guo, Q.; Wang, E. G. *J. Phys. Chem. B* **2005**, *109*, 4953.
(37) Borca, C. N.; Canulescu, S.; Loviat, F.; Lippert, T.; Grolimund, D.; Döbeli, M.; Wambach, J.; Wokaun, A. *Appl. Surf. Sci.* **2007**, *254*, 1352.

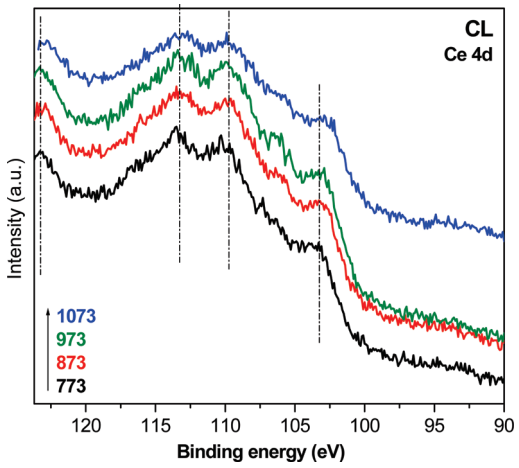

Figure 3. Ce 4d XP spectra of ceria-lanthana (CL) samples calcined at various temperatures from 773 to 1073 K.

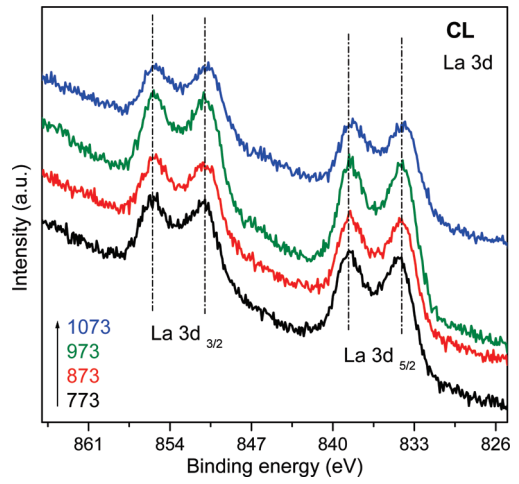

Figure 4. La 3d XP spectra of ceria-lanthana (CL) samples calcined at various temperatures from 773 to 1073 K.

noted, with increase of calcination temperature, there is no change in the intensity or position of the La 3d core level peaks.

The O 1s core level spectra of CL sample calcined at various temperatures and pure ceria calcined at 773 K resolved using Gaussian−Lorentzian model functions are presented in Figure 5. The curve fitted into two components, and the main peak at low binding energy (~529.4 eV) is corresponding to lattice oxygen. In fact, the charge on the oxide ions is significantly influenced by their surrounding chemical environment as a result peak shifts to either side depending upon the nature of the dopant ions. The shift gives an impression that the La^{3+} is combined with ceria to form a Ce—O—La type bond. The basic nature of La^{3+} may push the electron density toward oxide ion so that a chemical shift of −1.0 eV is apparent. This would induce the reduction of the Ce—O electrostatic attraction and result weakly bound oxygen which may further contribute to the OSC of ceria. The contribution from the high binding energy observed at ~531.8 eV ($\Delta E_B \cong 2.4$ eV) is attributed to surface hydroxyl groups and carbonates as these are confirmed by FTIR (~3425 cm^{-1}: O—H stretching) and the broadness

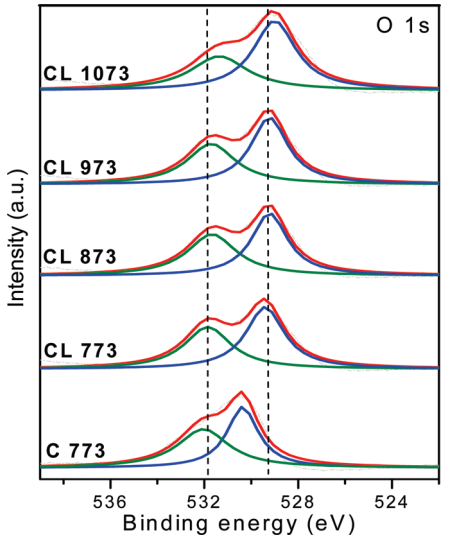

Figure 5. O 1s XP spectra of ceria-lanthana (CL) samples calcined at various temperatures from 773 to 1073 K.

Table 2. Binding Energy (eV) and Surface Composition of Ceria-Lanthana (CL) Calcined at Various Temperatures

	binding energy (eV)			surface composition	
sample	Ce 3d (u''')	La 3d (5/2)	O 1s	Ce	La
CeO_2 773	917.6		530.5	-	-
CeO_2−La_2O_3 773	917.1	834.4	529.5	57.4	42.5
CeO_2−La_2O_3 873	917.1	834.3	529.3	57.1	42.8
CeO_2−La_2O_3 973	916.5	834.0	529.2	57.5	42.4
CeO_2−La_2O_3 1073	917.0	833.8	529.2	56.5	43.4

observed in the C 1s core level spectra, respectively.[38,39] This peak intensity is more compared to pure ceria which stresses that CL contained more oxygen vacancies and is in a more reduced state.[34] The peak intensity is decreased due to removal of surface residues under thermal treatments. The surface compositions of Ce and La in CL sample calcined at various temperatures are given in the Table 2. It is observed that the content of La on the surface region is ~42% which is higher than that of the nominal content of 20%, while the content of Ce is ~57% which is lower than that of the nominal content of 80%. These results give an impression that the surface is slightly enriched with La^{3+}, a similar observation was also reported by Belliére et al.[27] However, with increase in calcination temperature there was no significant difference. The segregation of lanthana on the surface of sample is probably due to the difference in the hydrolysis rate and ionic radius of Ce^{4+} and La^{3+} ions.[40]

Raman spectroscopy is a useful technique to confer the information on the oxygen vacancies of oxide materials, especially ceria-containing solid solutions. The UV-RS results pertaining to CL sample calcined at various

(38) Borchert, H.; Frolova, Y. V.; Kaichev, V. V.; Prosvirin, I. P.; Alikina, G. M.; Lukashevich, A. I.; Zaikovskii, V. I.; Moroz, E. M.; Trukhan, S. N.; Ivanov, V. P.; Paukshtis, E. A.; Bukhtiyarov, V. I.; Sadykov, V. A. *J. Phys. Chem. B* **2005**, *109*, 5728.
(39) Xu, Q.; Heaton, B. T.; Jacob, C.; Mogi, K.; Ichihashi, Y.; Souma, Y.; Kanamori, K.; Eguchi, T. *J. Am. Chem. Soc.* **2000**, *122*, 6862.
(40) Mouzon, J. Synthesis of Yb:Y_2O_3 Nanoparticles and Fabrication of Transparent Polycrystalline Yttria Ceramics, Thesis submitted to Claude Bernard University, Lyon, France, 2005.

temperatures along with pure ceria calcined at 773 and 1073 K are shown in Figure 6. The corresponding Vis-RS of these samples are presented in Figure 7. RS of pure ceria exhibits one $F_{2\,g}$ band, generally centered at ~465 cm^{-1}, which can be viewed as symmetric breathing mode of the oxygen ions surrounded by the cations.[41] This band is sensitive to any disorder in the oxygen sublattice and the presence of this band indicates that La^{3+}-doped ceria exhibits a global cubic fluorite type structure. One more band observed at ~570 cm^{-1} is frequently characterized as nondegenerate longitudinal optical (LO) mode and is introduced due to charge compensation mechanism.[21] Although the CL Raman spectra resembled like pure ceria, several features can be highlighted. As ceria is doped with La^{3+}, the $F_{2\,g}$ mode becomes asymmetric and slightly shifted to lower wavenumber and the fwhm increased compared to pure ceria. This shift is the result of combined effects: decrement in the M—O vibrations as La^{3+} is introduced into ceria lattice (deformation takes place in the crystal structure due to larger ionic radius of La^{3+} compared to Ce^{4+}), lattice expansion, decrease in the crystallite size, and presence of oxygen vacancies.[16,42] $F_{2\,g}$ band shifting and absence of peak corresponding to La_2O_3 (generally observed at 405 cm^{-1}, attributed to torsional skeleton mode of hexagonal units) indicates the La^{3+} incorporation and formation of solid solution.[24,43] The increase of fwhm relative to pure ceria is apparently associated with the decrease in the crystallite size and increase in the oxygen vacancy concentration which is inline with XRD results. It is also observed that as calcination temperature increases there is no change in the $F_{2\,g}$ band position which indicates that these bands do not vary with the crystallite size. In the UV-RS (Figure 6), the observed high intensity band at 570 cm^{-1} for CL sample compared to pure ceria may be due to the combined effect of shorter excitation laser used in the measurement and the La^{3+} surface enrichment observed by the XPS measurements. If the excitation laser wavelength decreases from 632.5 to 325 nm, it is hard to obtain bulk information.[42] For the UV-Raman measurement, we have used 325 nm as the excitation laser hence it is surface sensitive. In addition, a slight La^{3+} surface enrichment is also observed in the compositions of Ce and La calculated using XPS core level peaks which is also inline with literature reports.[44,45] Hence, it can be stated that surface is essentially covered with La^{3+} (along with the oxygen vacancies).[44,45] Therefore, the band at ~570 cm^{-1} for CL sample is corresponding to more oxygen vacancy formation near the surface region in comparison to pure ceria. The resonance Raman enhancement may also influence the intensity of 570 cm^{-1} band. It is observed from the figure that the position of this band is influenced by neither dopant nor laser wavelength.

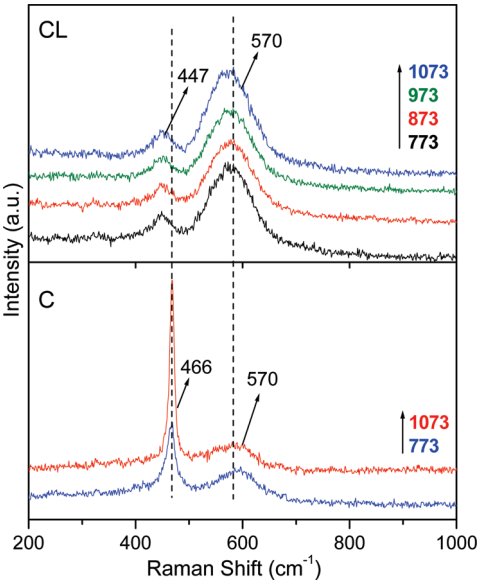

Figure 6. UV-Raman spectra of ceria (C) calcined at 773 and 1073 K and ceria-lanthana (CL) sample calcined at various temperatures from 773 to 1073 K.

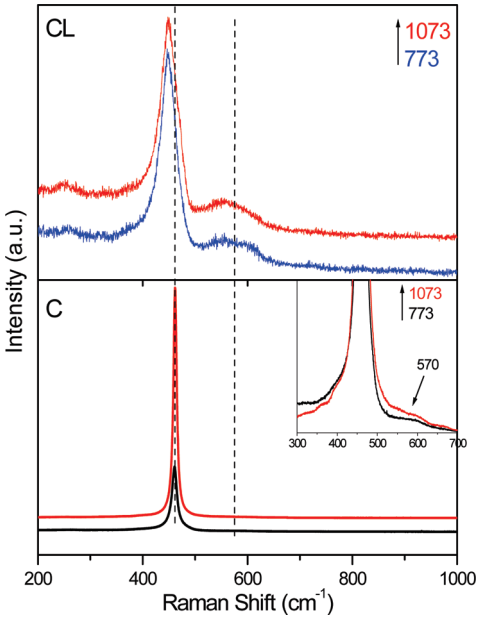

Figure 7. Vis-Raman spectra of ceria (C) and ceria-lanthana (CL) samples calcined at 773 and 1073 K.

To verify the results obtained from XRD and Raman measurements, TEM and HREM analyses were undertaken to monitor the morphological and structural changes and growth mechanism to confirm particle size and its shape during the thermal treatments. The corresponding micrographs of CL 773 and CL 1073 samples are shown in Figures 8 and 9, respectively. As can be seen from these figures, the shape of the particles at different calcination temperatures are cubic in nature (inset of Figure 8). It could be observed from the TEM-HREM images that the particles of the CL solid solutions are formed in uniform size and exhibit an average particle size

(41) Reddy, B. M.; Thrimurthulu, G.; Katta, L.; Yamada, Y.; Park, S.-E. *J. Phys. Chem. C* **2009**, *113*, 15882.
(42) Luo, M.-F.; Yan, Z.-L.; Jin, L.-Y.; He, M. *J. Phys. Chem. B* **2006**, *110*, 13068.
(43) Bueno-Lopez, A.; Krishna, K.; Makkee, M.; Moulijn, J. A. *J. Catal.* **2005**, *230*, 237.
(44) Wilkes, M. F.; Hayden, P.; Bhattacharya, A. K. *J. Catal.* **2003**, *219*, 295.
(45) Sayle, T. X. T.; Parker, S. C.; Catlow, C. R. A. *Surf. Sci.* **1994**, *316*, 329.

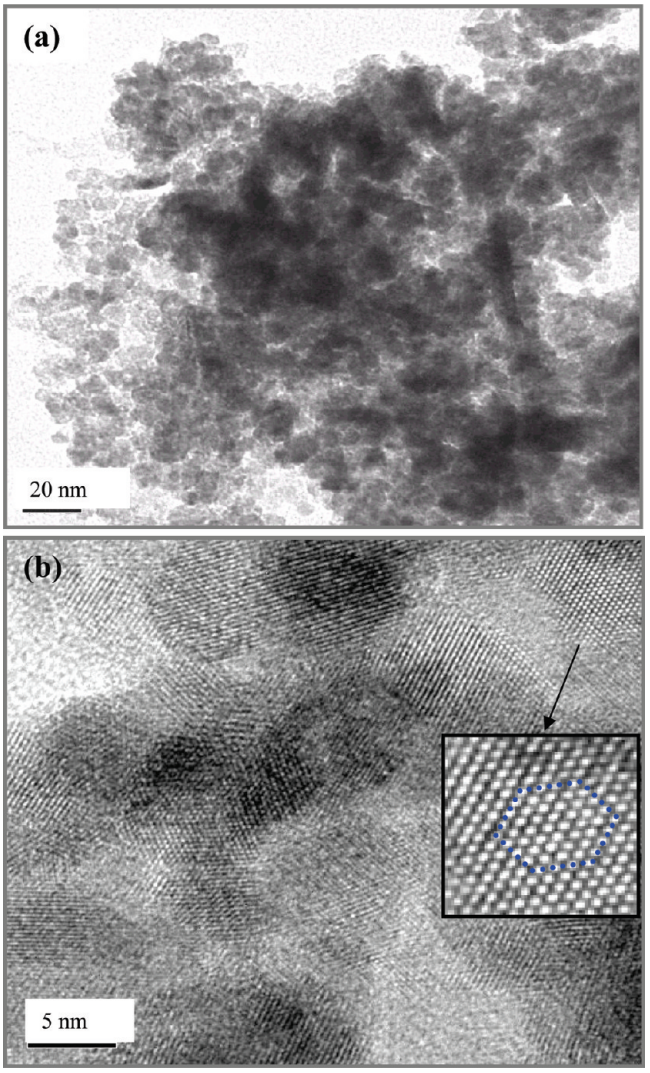

Figure 8. (a) TEM and (b) HREM images of ceria-lanthana (CL) sample calcined at 773 K (inset: enlarged views of selected areas).

of ~15 nm. Small particle size and narrow size distribution may be related to fast nucleation and slow growth process, which regulates the particle size of the catalyst.[46] With increase in the calcination temperature, morphology of the sample can be influenced, a gradual increase in the grain size is observed from ~7−8 to ~15 nm. These results quite agree well with the crystallite size data obtained from XRD using Scherrer equation (Table 1). The encircled area in the micrographs shows the closer view of the particles ensemble and orientation of the crystallographic planes during the heat treatment. As can be seen from the HREM images there are some overlapping regions of crystal planes, and some small steps observed. The existence of such overlapping regions and the steps in the mixed oxide particles are very important from the catalysis point of view, which may offer better catalytic activity.

UV-vis DRS technique is more useful to investigate the metal oxides with nanocrystalline nature which escape

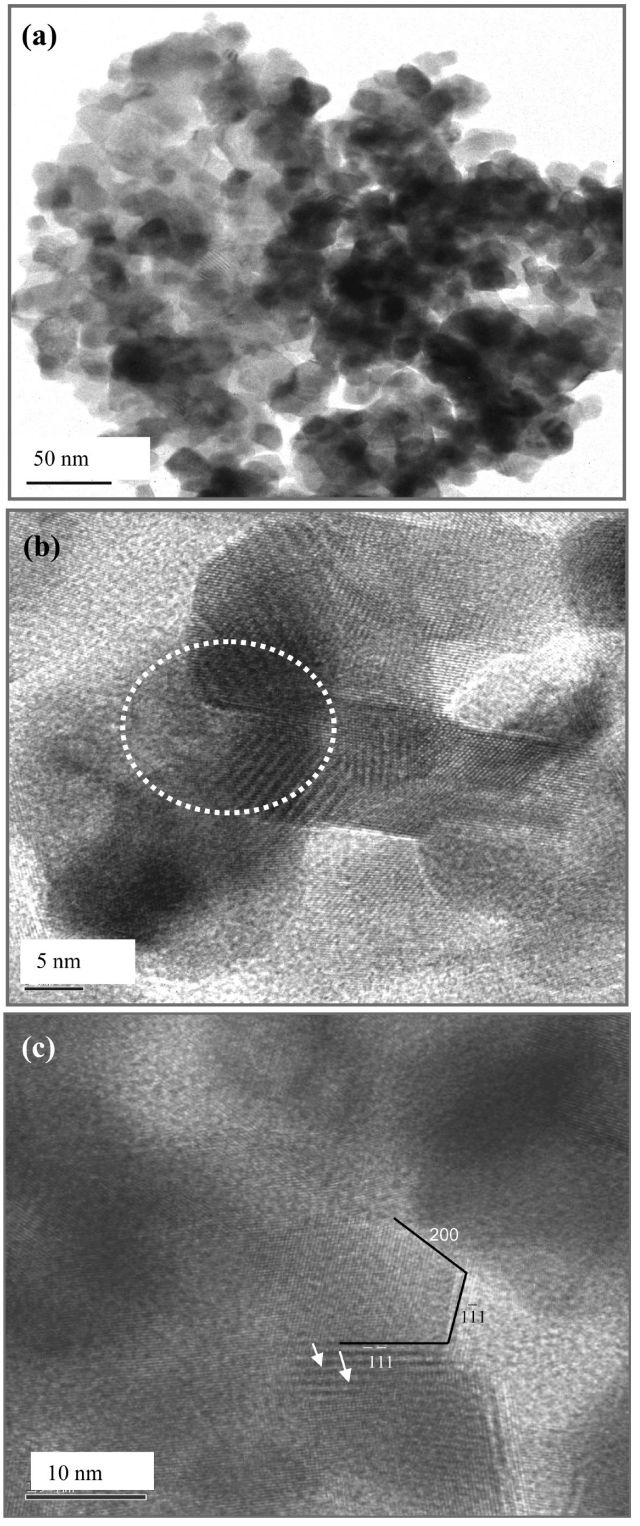

Figure 9. (a) TEM and (b) and (C) HREM images of ceria-lanthana (CL) sample calcined at 1073 K (inset: enlarged views of selected areas).

from the XRD detection.[47] There is no evidence for f-f or f-d transitions and crystal field transitions as La and Ce exhibit f^0 configuration in their respective stable oxidation states which are useful to obtain information regarding the coordination environment. Hence, the UV-vis

(46) Ramaswamy, V.; Haynes, T. E.; White, C. W.; Chan, W. J. M.; Roorda, S.; Aziz, M. J. *Nano. Lett.* **2005**, *5*, 373.

(47) Bensalem, A.; Bozon-Verduraz, F.; Delamar, M.; Bugli, G. *Appl. Catal., A* **1995**, *121*, 81.

DRS of ceria is originated mainly from charge-transfer transitions between O 2p and Ce 4f bonds. The representative spectra of CL sample calcined at 773 and 1073 K, and C calcined at 773 K are presented in Figure 10. A split of the absorption is observed at 255, 285, and 342 nm corresponding to the $O^{2-} \rightarrow Ce^{4+}$, $O^{2-} \rightarrow Ce^{3+}$ charge transfer (CT), and interband transitions (IBT) in the wavelength range of 250−340 nm.[47] The farmer band could be attributed to the defects created in the ceria lattice which is well resolved compared to the other two bands. Its presence also supports the appearance of the band at ∼570 cm^{-1} in RS measurements. There is no absorption band detected above 500 nm. From the figure, it is clear that La^{3+} doped ceria results in blue shift in the adsorption edge relative to pure ceria which could be explained based on the quantum confinement effect.[48]

Two consecutive steps are normally involved in the reduction process: the adsorption of H_2 results surface hydroxide groups on the oxide surface, and the ultimate oxygen vacancy formation takes place by recombination of these hydroxide groups.[49] The pure ceria undergoes reduction at ∼770 and ∼1100 K due to the surface and bulk reduction, respectively.[50] The difference in these two successive reduction temperatures are due to difference in their respective oxygen binding energies. The TPR plots of CL solid solution calcined at 773 and 1073 K are presented in Figure 11. As observed from the figure, the reduction temperatures for CL 773 and CL 1073 samples are 671 and 792 K, and 740 and 808 K, respectively, for the surface and bulk reductions. Doping of ceria with La^{3+} leads to shifting of reduction peaks toward lower temperature, and the total amount of desorbed oxygen from the CL sample is ∼1.5−2 times higher than the pure ceria. The low temperature surface reduction of CL is also partly attributed to increase in the surface area discussed in the later section. The mechanism of bulk reduction for both ceria and CL is same. However, the reason for low temperature bulk reduction of CL could be that the diffusion of bulk oxygen to the surface is relatively fast thus continuous flow of bulk oxide ions to the surface thereby creating more active sites on the surface for the adsorption of hydrogen.[51] Hence, an easy bulk reduction and significant appearance of bulk reduction peak are possible for the CL sample. With increase in the calcination temperature, shift of reduction peaks toward higher temperatures is due to decrease in the surface area (Table 1) despite the increase in the oxygen diffusion. Decrease in the surface is expected to reduce the number of active sites for the H_2 adsorption thereby its consumption can be decreased.

The specific surface area and OSC of CL samples calcined at various temperatures are shown in Table 1. As presented in Table 1, the surface area of CL sample is

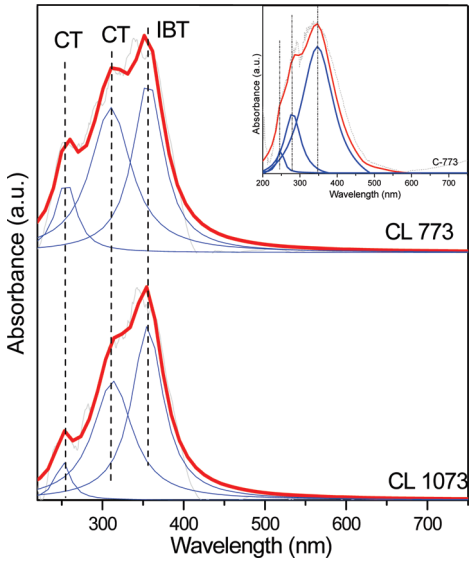

Figure 10. UV-vis DR spectra of ceria-lanthana (CL) samples calcined at 773 and 1073 K along with pure ceria (C) calcined at 773 K; (CT- charge transfer and IBT-inter band transition).

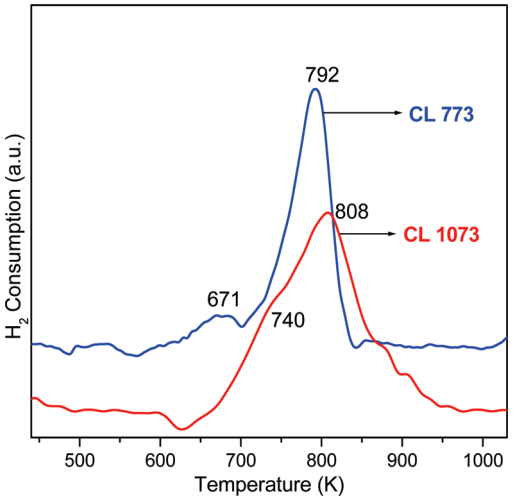

Figure 11. H_2 consumption as a function of temperature for ceria-lanthana (CL) sample calcined at 773 and 1073 K temperatures.

increased after the La^{3+} addition to ceria in agreement with the particle size decrease. Normally, high temperature treatment causes a gradual sintering and crystallite growth which leads to loss of surface area. However, the resistance to thermal sintering of these mixed oxides is significant in comparison to that of pure ceria. From Table 1 it is clear that the OSC of CL is increased by 4−5 times in comparison to pure ceria. This improved OSC may be credited to delocalized oxygen vacancies, weakly bound oxygen, and oxygen intestines in their defective crystal structures.[52] Addition of every two La^{3+} ions to ceria results one oxygen vacancy (extrinsic defect) by leaving two localized electrons into f-states of two Ce ions leading to Ce^{3+}.[50] Thus defects created during the incorporation of La^{3+} lead to ease of formation of labile oxygen vacancies, connected to this relatively high

(48) Sinha, A. K.; Suzuki, K. *J. Phys. Chem. B* **2005**, *109*, 1708.
(49) Bernal, S.; Blanco, G.; Cifredo, G.; Perez-Omil, J. A.; Pintado, J. M.; Izquierdo, J. M. R. *J. Alloys Comp.* **1997**, *250*, 449.
(50) Trovarelli, A. *Comments Inorg. Chem.* **1999**, *20*, 263.
(51) Daturi, M.; Finocchio, E.; Binet, C.; Lavalley, J. C.; Fally, F.; Perrichon, V. *J. Phys. Chem. B* **1999**, *103*, 4884.
(52) Mamontov, E.; Egami, T.; Brezny, R.; Koranne, M.; Tyagi, S. *J. Phys. Chem. B* **2000**, *104*, 11110.

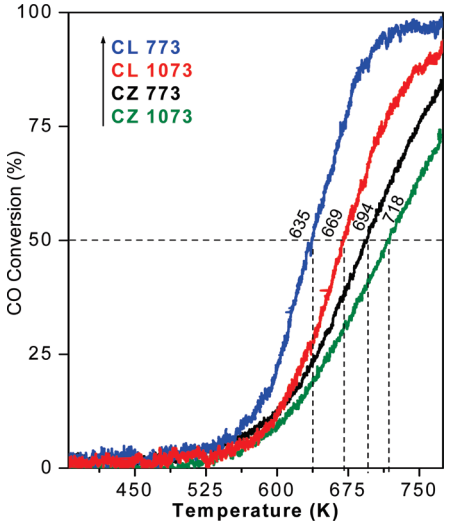

Figure 12. Conversion of CO (%) versus temperature (K) for ceria-lanthana (CL) and ceria-zirconia (CZ) samples calcined at 773 and 1073 K (up arrow indicates the increasing order of CO activity).

mobility of bulk oxygen species within the lattice cell thereby enhancement in the OSC.

We focused on the CO oxidation reaction which most likely to be affected by enhanced reducibility of the oxide solid solution. Figure 12 shows the typical activity curves of CO oxidation over Ce−La and Ce−Zr solid solutions calcined at 773 and 1073 K. Details pertaining to the structural characteristics of Ce−Zr solid solutions could be found elsewhere.[53] For better understanding of catalytic activity we highlighted the light-off temperatures ($T_{50\%}$; temperature where 50% conversion of CO takes place) in Figure 12. Both CL 773 and CL 1073 samples exhibited better activity compared to CZ 773 and CZ 1073 samples. The shapes of the CL curves revealed that conversion is very low at initial temperatures, increased at ca. 550 K (which could be sufficiently high to involve bulk oxygen) and approached 99% conversion below 744 K. Where as, the CZ upward curve started at 570 K and reached 84% conversion at 773 K. The $T_{50\%}$ is high even for CL 1073 sample compared to CZ 773 which further indicates the stability of CL sample at high calcination temperatures. The light-off temperatures of various catalysts followed the order: CL 773 < CL 1073 < CZ 773 < CZ 1073. The oxidation of CO on ceria occurs via Mars−van Krevelen redox type mechanism.[54] In the absence of feed, CO gets oxidized by consuming lattice oxygen and leaving the oxygen vacancy. In the presence of oxygen feed, the lattice oxygen is replenished.[55] Therefore, in the oxidation process lattice oxygen, conversely an oxygen vacancy, is involved and acts as an active site for the dissociation of gaseous oxygen. Accordingly, in the oxidation process vacancy plays an essential role.

From Raman and UV-vis DRS studies, formation of defect crystal structure with oxygen vacancies was observed which facilitate better catalytic activity for the mixed oxides. The slight La^{3+} enrichment on the surface may also contribute to the enhanced activity. The OSC is another parameter for the observed better conversion of CO. As observed from TPR, the CL sample undergoes easy reduction showing ample availability of lattice oxygen species to react with the adsorbed CO for giving high conversion.

4. Conclusions

We have synthesized $Ce_{1-x}La_xO_{2-\delta}$ ($x = 0.2$) solid solution by a simple and efficient way. Variation in the lattice parameter of CeO_2 has been ascribed to La^{3+} substitution and the formation of solid solution. Multioxidation states for Ce, and segregation of La^{3+} are observed from the XPS measurements. The presence of Ce^{3+} and concomitant O vacancies in the solid solution has been confirmed by Raman and XPS measurements. Raman measurements further disclosed the formation of Ce—La-oxides with fluorite type cubic structure with one deformed F_{2g} band and an additional band attributed to the oxygen vacancies. Crystallite size of the Ce—La solid solution was observed to be below 15 nm as revealed by XRD and HREM measurements. The specific surface area of the Ce—La solid was also found to be reasonably high. The UV-vis DRS measurements provided information regarding ligand to metal charge transfer transitions. Three significant experimental observations were mainly noticed from this study pertaining to the La^{3+} doped ceria: (a) an easy reduction and more H_2 consumption, (b) OSC is about 4−5 times more compared to pure ceria, and (c) light-off temperature of CL 773 for CO oxidation is lowered by around 58 K compared to CZ 773 solid solution. Thus, the combined use of different sophisticated techniques provided interesting key information pertaining to enhanced CO oxidation activity and high thermal stability of ceria-lanthana solid solutions.

Acknowledgment. We greatly acknowledge Prof. Dr. W. Grünert, RUB, Germany and Prof. S.-E. Park, Inha University, South Korea for providing CO oxidation and UV-Raman results, respectively. We also thank Dr. Tetsuo Umegaki, AIST-Kansai, Japan for help in XPS measurements. L.K. and G.T. wish to thank the Council of Scientific and Industrial Research (CSIR), New Delhi, for senior research fellowships.

(53) Reddy, B. M.; Bharali, P.; Saikia, P.; Park, S.-E.; van den Berg, M. W. E.; Muhler, M.; Grünert, W. *J. Phys. Chem. C* **2008**, *112*, 11729.
(54) Boaro, M.; de Leitenburg, C.; Dolcetti, G.; Trovarelli, A. *J. Catal.* **2000**, *193*, 338.
(55) Shapovalov, V.; Metiu, H. *J. Catal.* **2007**, *245*, 205.